(Preprint) AAS 16-151

OBSERVATIONS ON THE GEOMETRY OF HORIZON-BASED OPTICAL NAVIGATION

John Christian* **and Shane Robinson†**

NASA's Orion Project has sparked a renewed interest in horizon-based optical navigation (OPNAV) techniques for spacecraft in the Earth-Moon system. Some approaches have begun to explore the geometry of horizon-based OPNAV and exploit the fact that it is a conic section problem. Therefore, the present paper focuses more deeply on understanding and leveraging the various geometric interpretations of horizon-based OPNAV. These results provide valuable insight into the fundamental workings of OPNAV solution methods, their convergence properties, and associated estimate covariance. Most importantly, the geometry and transformations uncovered in this paper lead to a simple and non-iterative solution to the generic horizon-based OPNAV problem. This represents a significant theoretical advancement over existing methods. Thus, we find that a clear understanding of geometric relationships is central to the prudent design, use, and operation of horizon-based OPNAV techniques.

INTRODUCTION

Optical navigation (OPNAV) using the lit horizon of a planet or moon has received considerable attention over the past few decades for both robotic and human spaceflight. Recently, the Orion program has investigated the use of horizon-based OPNAV to allow the crew to autonomously navigate back to Earth in the event of a communication system failure. This application has created a need for improved performance of horizon-based methods, which has resulted in new work by both Christian[1–4] and Mortari[5,6] in the past few years. Given the proliferation of new methods and results, we felt it was important to more deeply study and document the rich geometry of the generic horizon-based OPNAV problem.

Although the bulk of this paper is dedicated to a more thorough understanding of horizon-based OPNAV geometry, our study of this topic has unlocked an exact and non-iterative solution for navigation relative to an ellipsoidal planet. This represents a significant advancement in the theory of horizon-based OPNAV, as previous approaches have been iterative, approximate, or both. Our new solution is presented towards the end of the paper, just prior to the numerical results.

OPNAV GEOMETRY FUNDAMENTALS

Horizon-based OPNAV is a conic section problem.[3] If the planet is modeled as a triaxial ellipsoid, then the apparent horizon is formed by the rays emanating from the camera that are tangent to the planet surface. The collection of all of these rays forms a cone that tightly bounds the planet with its vertex located at the camera optical center. The perspective projection of the horizon is formed by taking a planar slice of this cone with the image plane. Thus, the apparent horizon of an ellipsoidal planet in an image is formed by a conic section — and is found to be an ellipse in all reasonable OPNAV scenarios. This is all shown graphically in Fig. 1. We now review the fundamental relations that govern OPNAV geometry in more detail.

*Assistant Professor, Department of Mechanical and Aerospace Engineering, West Virginia University, Morgantown, WV 26506.
†Aerospace Engineer, Aeroscience and Flight Mechanics Division, NASA Johnson Space Center, 2101 NASA Parkway, Houston TX 77058.

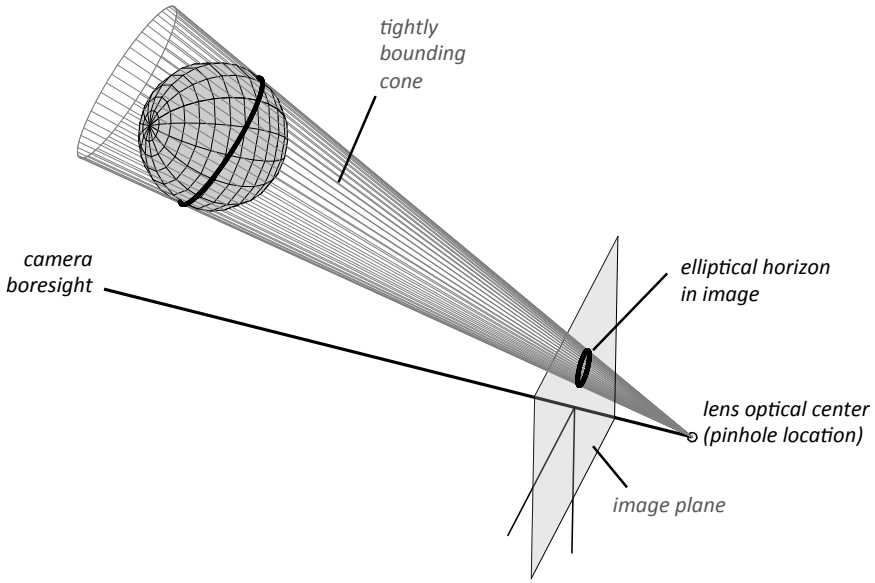

Figure 1. Geometry of horizon-based OPNAV as a conic section.

Perspective Projection and the Pinhole Camera Model

Ideal image formation is governed by perspective projection and can be described by the pinhole camera model. Although real cameras are not pinholes and suffer from an assortment of distortions and imperfections, these may be accounted for via calibration to produce a result functionally equivalent to a pinhole camera.[7]

Therefore, we proceed with the standard description of the pinhole camera,[8]

$$x = f\frac{X}{Z} \qquad y = f\frac{Y}{Z} \tag{1}$$

where f is the focal length, $[X, Y, Z]$ are a point's 3D coordinates in the camera frame and $[x, y]$ are the coordinates of the perspective projection of that point onto the image plane. We define the camera frame to have it's origin at the camera's optical center (the pinhole location) with $+Z$ pointing along the bore-sight of the camera. Thus, any point observed by the camera will have a positive Z component. We also operate on the image plane instead of the focal plane to avoid unnecessarily dealing with a flipped image.

Without loss of generality, we often choose to work in focal length normalized coordinate and simply set $f = 1$ to arrive at

$$x = X/Z \qquad y = Y/Z \tag{2}$$

We can also write the image plane coordinate in terms of homogeneous coordinates,

$$\begin{bmatrix} x \\ y \\ 1 \end{bmatrix} = \frac{1}{Z}\begin{bmatrix} X \\ Y \\ Z \end{bmatrix} \tag{3}$$

which makes it apparent that the image plane coordinates occur at the place where the vector from the camera frame origin to the 3D point pierces the image plane (which is just the $Z = 1$ plane). Conversely, any point in an image may be used to form a ray which starts at the origin, passes through the point in the image plane, and then emanates out of the camera in this direction.

Apparent Horizon Location is Formed by a Conic Section

Let's begin by assuming that the planet or moon to be used for OPNAV may be reasonably modeled as a triaxial ellipsoid. The surface of an ellipsoid is described by the quadratic form

$$\mathbf{p}^T\mathbf{A}\mathbf{p} = 1 \tag{4}$$

where $\mathbf{A}$ is a 3×3 symmetric, positive definite matrix and $\mathbf{p}$ is point in the ellipsoidal surface with an origin at the planet's center.

With such a planet model, the points in the image belonging to the apparent horizon correspond to rays that start at the camera frame origin, emanate out of the camera, and are exactly tangent to the ellipsoidal planet's surface. This family of rays clearly forms a conical surface (again, see Fig. 1). Consequently, the apparent location of the horizon in an image is formed by taking a slice of this cone with the $Z = 1$ plane and is clearly a conic section problem. We now explore the mathematics of this in a bit more detail.

Suppose we have a camera viewing an ellipsoidal planet from a relative position of $\mathbf{r}$ (as expressed in the camera frame). We know that any particular ray, $\mathbf{s}_i$, belonging to the cone that tightly bounds the ellipsoidal planet obeys the constraint[3]

$$\mathbf{s}_i^T\mathbf{M}\mathbf{s}_i = 0 \tag{5}$$

where

$$\mathbf{M} = \mathbf{A}\mathbf{r}\mathbf{r}^T\mathbf{A} - (\mathbf{r}^T\mathbf{A}\mathbf{r} - 1)\mathbf{A} \tag{6}$$

and $\mathbf{M}$ is a symmetric 3×3 matrix of full rank. For the special case of a spherical planet, where $\mathbf{A} = a\,\mathbf{I}_{3\times3}$, we observe that $\mathbf{M}$ collapses to simply

$$\mathbf{M} = a^2\mathbf{r}\mathbf{r}^T - a(a\mathbf{r}^T\mathbf{r} - 1)\mathbf{I}_{3\times3} \tag{7}$$

$$\mathbf{M} = a^2\,[\mathbf{r}\times]\,[\mathbf{r}\times] + a\,\mathbf{I}_{3\times3} \tag{8}$$

where $[\,\cdot\,\times]$ is the skew-symmetric cross product matrix, such that $[\boldsymbol{\alpha}\times]\,\boldsymbol{\beta} = \boldsymbol{\alpha} \times \boldsymbol{\beta}$.

Because the constraint in Eq. 6 is satisfied for all points existing on the planet's tightly bounding cone, it satisfied for the points that lie on the intersection of this cone with the image plane (the $Z = 1$ plane). Thus, we may parameterize $\mathbf{s}_i$ in terms of only the ray's coordinates in the 2D image plane, $\{x_i, y_i\}$. That is, $\mathbf{s}_i^T = \begin{bmatrix} x_i & y_i & 1 \end{bmatrix}$. Substituting this into Eq. 5 and expanding in terms of the individual entries in $\mathbf{M}$,

$$\mathbf{s}_i^T\mathbf{M}\mathbf{s}_i = m_{11}x_i^2 + 2m_{12}x_iy_i + 2m_{13}x_i + m_{22}y_i^2 + 2m_{23}y_i + m_{33} = 0 \tag{9}$$

which is a generic 2D quadratic curve, and we recall that the non-degenerate quadratics are simply the conic sections (circle, ellipse, parabola, or hyperbola). To make things a bit simpler, we apply the following variable substitutions

$$A = m_{11} \qquad B = 2m_{12} \qquad C = m_{22} \tag{10}$$

$$D = 2m_{13} \qquad F = 2m_{23} \qquad G = m_{33}$$

which leads us to the standard implicit equation for a conic section,

$$Ax_i^2 + Bx_iy_i + Cy_i^2 + Dx_i + Fy_i + G = 0 \tag{11}$$

If $4AC > B^2$ then the conic section is an ellipse. We will now demonstrate that the conic section must be an ellipse for all practical OPNAV scenarios.

Usable OPNAV Images have an Elliptical Horizon

In general, it is possible to for a horizon to appear as an ellipse (or circle), parabola, or hyperbola. Parabolic and hyperbolic horizons, however, are only possible at very close ranges where an insufficient amount of horizon arc is present for precision OPNAV. Thus, we typically encounter elliptical horizons in practice.

For the conic section to be an ellipse, the entirety of the intersection between the image plane and the planet's tightly bounding cone must be on the half of the cone containing the planet. For a spherical planet, this means the planet's center must be a distance of at least the planet's radius in front of the camera.

Recall that the ellipse constraint is $4AC > B^2$. That is, we seek the condition where

$$4AC - B^2 > 0 \tag{12}$$

or, after some substitution from above,

$$4AC - B^2 = a^2 \left(az_i^2 - 1\right) \left[a(x_i^2 + y_i^2 + z_i^2) - 1\right] > 0 \tag{13}$$

Since $a = 1/r_p^2$ (where r_p is the planet radius), the right-most term will always be greater than zero. The only way for this term to be less than zero would be for the camera to be located inside the planet. Thus, the constraint of importance is

$$(z_i/r_p)^2 > 1 \tag{14}$$

Which simply states that the z-component of the relative position between the camera and the planet center must be greater than the planet's radius.

Given the constraint in Eq. 14, it also is possible to determine above which altitudes only an ellipse is possible with a camera of a specified field-of-view (FOV). The transition occurs where the angle between the focal plane and the direction to the planet center is the same as the cone half angle, as shown in Fig. 2. Note that this occurs at exactly the point where the z-component of $\mathbf{r}$ is exactly r_p, which is a purely geometric way of arriving at the same result as in Eq. 14.

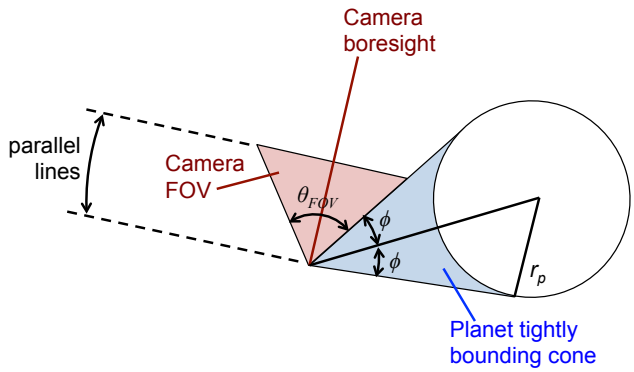

Figure 2. Geometry when a parabolic horizon first becomes possible.

For the horizon to be elliptical, the image plane must intersect the tightly bounding cone entirely on the same side of the cone while also having the horizon in the FOV. Since the transition point between a closed and open conic section is a parabola, we seek the range and FOV combination where a parabolic horizon first becomes possible. Thus, as can be seen in Fig. 2, a parabolic or hyperbolic horizon may occur whenever the following inequality is satisfied:

$$2\phi + \theta_{FOV}/2 \geq \pi/2 \tag{15}$$

where ϕ is the cone half angle and θ_{FOV} is the camera full FOV. The above inequality may be rewritten as

$$\phi \geq \pi/4 - \theta_{FOV}/4 \tag{16}$$

Now, recognizing that

$$\sin\phi = r_p/\rho \tag{17}$$

where ρ is the range to the planet. Since $\phi \leq \pi/2$, we know that $\sin(\phi) \geq \sin(\pi/4 - \theta_{FOV}/4)$. Therefore, a parabolic or hyperbolic horizon may occur when

$$\rho \leq \frac{r_p}{\sin\left(\pi/4 - \theta_{FOV}/4\right)} \tag{18}$$

This same final result was first presented in [3]. At ranges greater than this, only an elliptical horizon is possible. At ranges less than this, parabolic and hyperbolic horizons are also possible.

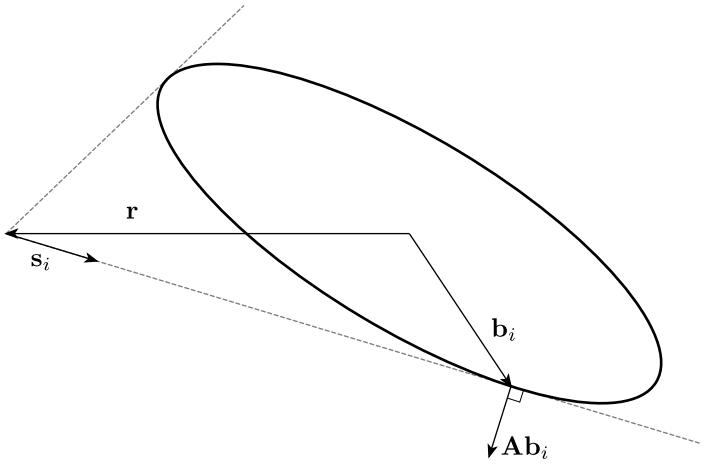

Figure 3. Geometry of position to limb measurements for an ellipsoidal planet.

SQUARE ROOT FACTORIZATION SPACE

Although the problem geometry is straightforward for an ellipsoidal planet, it becomes especially intuitive for a spherical planet. Furthermore, things become even simpler if the planet is a unit sphere — that is, when when $\mathbf{A} = \mathbf{I}$. We now show that the square root factorization provides a mechanism to transform horizon-based OPNAV with respect to an arbitrary ellipsoidal planet into this idealized geometry.

To begin, combine Eq. 5 and Eq. 6,*

$$\mathbf{s}_i^T \underbrace{\left[\mathbf{A}\mathbf{r}\mathbf{r}^T\mathbf{A} - \left(\mathbf{r}^T\mathbf{A}\mathbf{r} - 1\right)\mathbf{A}\right]}_{\mathbf{M}} \mathbf{s}_i = 0 \tag{19}$$

As shown in [3], this equation can be manipulated to yield

$$\mathbf{s}_i^T\mathbf{A}\mathbf{s}_i = \mathbf{r}^T\left[\left(\mathbf{s}_i^T\mathbf{A}\mathbf{s}_i\right)\mathbf{A} - \mathbf{A}\mathbf{s}_i\mathbf{s}_i^T\mathbf{A}\right]\mathbf{r} \tag{20}$$

While this equation is tantalizing, the beauty of it's intrinsic geometry is more fully revealed by transforming to a square root factorization space. As will be seen, this transformation provides significant insight and utility.

Proceed by dividing the above equation by the scalar $\mathbf{s}_i^T\mathbf{A}\mathbf{s}_i$

$$1 = \mathbf{r}^T\left[\mathbf{A} - \frac{\mathbf{A}\mathbf{s}_i\mathbf{s}_i^T\mathbf{A}}{\mathbf{s}_i^T\mathbf{A}\mathbf{s}_i}\right]\mathbf{r} \tag{21}$$

*Depite the present application being limited to 3 dimensions, the development here is valid for n dimensions.

Here the projective structure of the equation begins to be uncovered. Application of the square root factorization makes the projective structure much more obvious. Here we use an upper triangular Cholesky factorization, $\mathbf{A} = \mathbf{U}^T\mathbf{U}$, but this same approach will work with any valid invertible square root matrix of $\mathbf{A}$.

$$1 = \mathbf{r}^T\mathbf{U}^T \left[\mathbf{I} - \frac{\mathbf{U}\mathbf{s}_i\mathbf{s}_i^T\mathbf{U}^T}{\mathbf{s}_i^T\mathbf{U}^T\mathbf{U}\mathbf{s}_i}\right] \mathbf{U}\mathbf{r} \tag{22}$$

Cleanup the equation by representing in the vectors in the square root factorized space. This is done by substituting $\bar{\mathbf{r}} = \mathbf{U}\mathbf{r}$ and $\bar{\mathbf{s}}_i = \mathbf{U}\mathbf{s}_i$

$$1 = \bar{\mathbf{r}}^T \left[\mathbf{I} - \frac{\bar{\mathbf{s}}_i\bar{\mathbf{s}}_i^T}{\bar{\mathbf{s}}_i^T\bar{\mathbf{s}}_i}\right] \bar{\mathbf{r}} \tag{23}$$

Now, the last term can be written as the product of of the unit vector $\bar{\mathbf{s}}_i^{'} = {}^{\bar{\mathbf{s}}_i}/_{\|\bar{\mathbf{s}}_i\|}$

$$1 = \underbrace{\bar{\mathbf{r}}^T \left[\mathbf{I} - \bar{\mathbf{s}}_i^{'}\bar{\mathbf{s}}_i^{'T}\right]}_{\bar{\mathbf{b}}_i^{'T}} \bar{\mathbf{r}} \tag{24}$$

Where $\bar{\mathbf{b}}_i^{'}$ is easily shown to be a unit vector. Now the projective geometry shown in Fig. 4 is clear. This equation can be rewritten as an inner product of two vectors

$$1 = \bar{\mathbf{b}}_i^{'T}\bar{\mathbf{r}} = \bar{\rho}\cos\left(\bar{\theta}\right) \tag{25}$$

where $\bar{\rho} = |\bar{\mathbf{r}}|$ is the range. Note that in the square root factorized space $\bar{\theta}$ and is the same for all i.

An alternative perspective is possible by noting that Eq. 24 can be written as

$$1 = \bar{\mathbf{r}}^T \underbrace{\left[\bar{\mathbf{s}}_i^{'}\times\right]^T \left[\bar{\mathbf{s}}_i^{'}\times\right]}_{\mathbf{S}_i} \bar{\mathbf{r}} \tag{26}$$

This leads directly to two useful relations

$$\bar{\mathbf{b}}_i = -\bar{\mathbf{s}}_i^{'} \times \left(\bar{\mathbf{s}}_i^{'} \times \bar{\mathbf{r}}\right) \tag{27}$$

$$1 = \left\|\bar{\mathbf{s}}_i^{'} \times \bar{\mathbf{r}}\right\| = \bar{\rho}\sin\left(\bar{\phi}\right) \tag{28}$$

Again note that $\bar{\mathbf{b}}_i^{'}$ is easily shown to be a unit vector and that $\bar{\phi}$ is a constant in the square root factorized space.

The square root factorization offers powerful insight and utility. By providing a transformation from any problem into the simplest problem (i.e. the unit sphere), any relationship available in the unit sphere problem now becomes applicable to the original problem — even if the original problem involves an arbitrary elliptic planet. Leveraging this newfound insight unlocks a multitude of new approaches to various aspects of the horizon-based OPNAV problem. Perhaps most significantly, it provides a path to and elegant non-iterative solution. Before developing the non-iterative solution, the geometry of iterative solutions is understood by applying the square root factorization.

GEOMETRY OF CONVERGENCE FOR ITERATIVE METHODS

Given n horizon measurements, various iterative methods exist for finding the solution to the OPNAV problem. The first method is to use fixed point iteration to find the value of $\bar{\mathbf{r}}$ which minimizes the square of the errors.[3] This is accomplished by iteratively finding the least squares solution to the system of linear

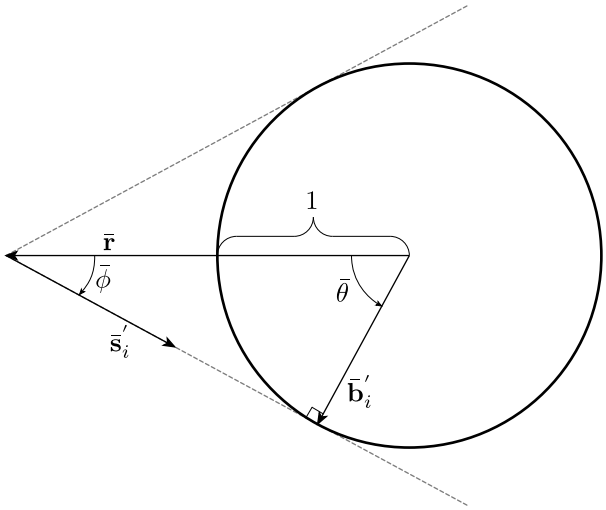

Figure 4. Geometry of position to limb measurements for an ellipsoidal planet.

equations

$$\begin{bmatrix} 1 \\ 1 \\ \vdots \\ 1 \end{bmatrix} = \begin{bmatrix} \hat{\bar{\mathbf{b}}}_1^T \\ \hat{\bar{\mathbf{b}}}_2^T \\ \vdots \\ \hat{\bar{\mathbf{b}}}_n^T \end{bmatrix} \hat{\bar{\mathbf{r}}}_{(+)} \tag{29}$$

where $\hat{\bar{\mathbf{b}}}_i = \hat{\bar{\mathbf{r}}}_{(-)}^T \mathbf{S}_i$ and $\hat{\bar{\mathbf{r}}}$ is an estimate of the position. The least squares solution to Eq. 29 is

$$\hat{\bar{\mathbf{r}}}_{(+)} = \left[\sum_{k=1}^{n} \mathbf{S}_i \hat{\bar{\mathbf{r}}}_{(-)} \hat{\bar{\mathbf{r}}}_{(-)}^T \mathbf{S}_i \right]^{-1} \left[\sum_{k=1}^{n} \mathbf{S}_i \right] \hat{\bar{\mathbf{r}}}_{(-)} \tag{30}$$

Naïvely solving this problem using a fixed point iteration scheme will lead to a strong oscillatory behavior in the solution and poor convergence — a fact that was earlier observed by Christian.[3] We now present a novel and geometric way of understanding this oscillatory behavior using the square root factorized space.

Observe that $\hat{\bar{\mathbf{b}}}_i$ is only a unit vector when $\hat{\bar{\mathbf{r}}}$ lies on the line of sight.

$$\left\| \hat{\bar{\mathbf{b}}}_i \right\| = \hat{b}_i \neq 1 \tag{31}$$

This means that each line of the above equation can be written

$$1 = \hat{\bar{\mathbf{b}}}_i^T \hat{\bar{\mathbf{r}}}_{(+)} = \hat{b}_i \ \left\| \hat{\bar{\mathbf{r}}}_{(+)} \right\| \cos\left(\bar{\theta}\right) \tag{32}$$

Presume that over one iteration $\bar{\theta}$ remains constant. Which is reasonable as the direction of $\hat{\bar{\mathbf{r}}}$ should remain relatively constant.

$$1/\,\hat{b}_i = \left\| \hat{\bar{\mathbf{r}}}_{(+)} \right\| \cos\left(\bar{\theta}\right) \tag{33}$$

For near unitary values of $\hat{b}_i$

$$\varepsilon_i = 1 - \hat{b}_i \approx 1/\,\hat{b}_i - 1 \tag{34}$$

The associated geometry is shown in figure 5. This shows the cause of the strong oscillatory behavior observed in a naïve fixed point iteration scheme to be rooted deep within the geometry of the problem.

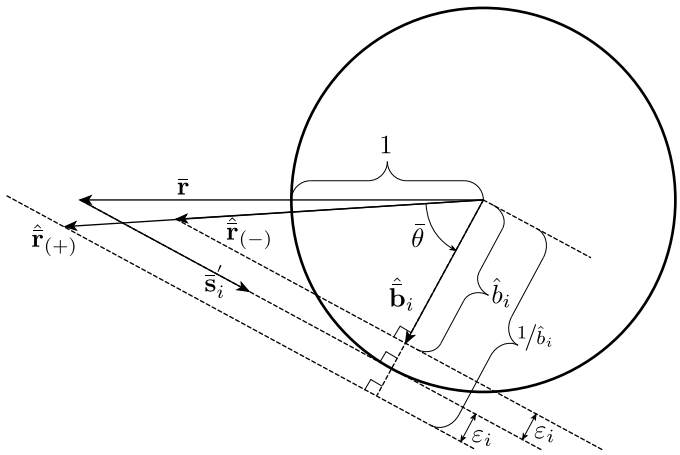

Figure 5. Geometry associated with convergence oscillations.

Equation 34 correctly suggests that the oscillatory behavior can be resolved by averaging the current estimate with the previous estimate. This is exactly the solution suggested by Christian's *Iterative Horizon Reprojection* (IHR) method[3]

$$\hat{\bar{\mathbf{r}}}_{(+)} = \frac{1}{2}\left(\mathbf{I} + \left[\sum_{k=1}^{n} \mathbf{S}_i \hat{\bar{\mathbf{r}}}_{(-)} \hat{\bar{\mathbf{r}}}_{(-)}^T \mathbf{S}_i\right]^{-1} \left[\sum_{k=1}^{n} \mathbf{S}_i\right]\right) \hat{\bar{\mathbf{r}}}_{(-)} \tag{35}$$

One minor augmentation that would help convergence would be to enforce $\left\|\hat{\bar{\mathbf{b}}}_i\right\| = \hat{b}_i = 1$.

Here, a third solution path is suggested which uses a Newton-Raphson iteration to solve the least squares problem directly. The sum of the squared error for Eq. 26 is

$$J = \frac{1}{4}\sum_{k=1}^{n} \left(\hat{\bar{\mathbf{r}}}^T \mathbf{S}_i \hat{\bar{\mathbf{r}}} - 1\right)^2 \tag{36}$$

The intent of least squares is to find $\hat{\bar{\mathbf{r}}}$ which minimizes this quantity. This is done by selecting a value of $\hat{\bar{\mathbf{r}}}$ which corresponds to a gradient of zero. The needed gradient is supplied by finding the partial with respect to $\hat{\bar{\mathbf{r}}}$

$$\frac{\partial J}{\partial \hat{\bar{\mathbf{r}}}^T} = \sum_{k=1}^{n} \left(\hat{\bar{\mathbf{r}}}^T \mathbf{S}_i \hat{\bar{\mathbf{r}}} - 1\right) \mathbf{S}_i \hat{\bar{\mathbf{r}}} \tag{37}$$

A value of $\hat{\bar{\mathbf{r}}}$ which drives this vector to zero will correspond to an extremum of Eq. 36. In order to solve this problem using Newton-Raphson iteration the Hessian is needed

$$\frac{\partial^2 J}{\partial \hat{\bar{\mathbf{r}}}^T \partial \hat{\bar{\mathbf{r}}}} = \sum_{k=1}^{n} \left[2\mathbf{S}_i \hat{\bar{\mathbf{r}}} \hat{\bar{\mathbf{r}}}^T \mathbf{S}_i + \left(\hat{\bar{\mathbf{r}}}^T \mathbf{S}_i \hat{\bar{\mathbf{r}}} - 1\right) \mathbf{S}_i\right] \tag{38}$$

Thus, the Newton-Raphson iterate is

$$\hat{\bar{\mathbf{r}}}_{(+)} = \hat{\bar{\mathbf{r}}}_{(-)} - \left[\sum_{k=1}^{n} \left[2\mathbf{S}_i \hat{\bar{\mathbf{r}}}_{(-)} \hat{\bar{\mathbf{r}}}_{(-)}^T \mathbf{S}_i + \left(\hat{\bar{\mathbf{r}}}_{(-)}^T \mathbf{S}_i \hat{\bar{\mathbf{r}}}_{(-)} - 1\right) \mathbf{S}_i\right]\right]^{-1} \left[\sum_{k=1}^{n} \left(\hat{\bar{\mathbf{r}}}_{(-)}^T \mathbf{S}_i \hat{\bar{\mathbf{r}}}_{(-)} - 1\right) \mathbf{S}_i \hat{\bar{\mathbf{r}}}_{(-)}\right] \tag{39}$$

Using the matrix inversion lemma this can be written

$$\hat{\bar{\mathbf{r}}}_{(+)} = \left(\mathbf{I} + \frac{1}{2}\left[\sum_{k=1}^{n} \mathbf{S}_i \hat{\bar{\mathbf{r}}}_{(-)} \hat{\bar{\mathbf{r}}}_{(-)}^T \mathbf{S}_i\right]^{-1} \left[\sum_{k=1}^{n} \left(\hat{\bar{\mathbf{r}}}_{(-)}^T \mathbf{S}_i \hat{\bar{\mathbf{r}}}_{(-)} - 1\right) \mathbf{S}_i\right]\right)^{-1} \hat{\bar{\mathbf{r}}}_{(-)} \tag{40}$$

Once the solution is found in the square root factorization space it must be transformed back to the original space,

$$\mathbf{r} = \mathbf{U}^{-1}\bar{\mathbf{r}} \tag{41}$$

The upper triangular, diagonally dominant structure of $\mathbf{U}$ insures that this operation is well conditioned.

We find that the two non-oscillatory methods (IHR and Newtwon-Raphson iteration) have very nearly the same convergence properties. Although which technique converges fastest depends on the specific situation, the residuals as a function of iteration number are almost always of the same order between the two methods. A detailed discussion of the convergence properties of IHR are provided in [3].

NON-ITERATIVE HORIZON-BASED OPNAV

As was mentioned earlier, transforming a horizon-based OPNAV problem into square root factorized space turns every problem into navigation relative to a unit sphere. This is true even for very elliptical planets. Fortunately, this simpler geometry admits a non-iterative solution. Since the planet becomes a sphere in the transformed space, its tightly bounding cone is a right-circular cone. Thus, in square root factorized space, the angle between every horizon line-of-sight direction and the relative position vector (which coincides with cone centerline for a sphere) is the same,

$$\bar{\mathbf{s}}_i^{'T}\bar{\mathbf{r}} = -\|\bar{\mathbf{s}}_i^{'}\|\,\|\bar{\mathbf{r}}\|\cos\left(\bar{\phi}\right) \tag{42}$$

where the negative sign comes from the fact that $\bar{\mathbf{r}}$ goes from the center of the planet to the spacecraft. Define $\bar{\rho} = \|\bar{\mathbf{r}}\|$ as the range in square root factorized space and $\mathbf{e} = \bar{\mathbf{r}}/\bar{\rho}$. Therefore, recalling that $\bar{\mathbf{s}}_i^{'}$ is a unit vector, we obtain

$$\bar{\mathbf{s}}_i^{'T}\mathbf{e} = -\cos\left(\bar{\phi}\right) \tag{43}$$

Thus, defining $\mathbf{n}$ as

$$\mathbf{n} = -\left(\frac{1}{\cos\left(\bar{\phi}\right)}\right)\mathbf{e} \tag{44}$$

we obtain the following relation for each horizon measurement

$$\bar{\mathbf{s}}_i^{'T}\mathbf{n} = 1 \tag{45}$$

Figure 6 shows the geometric meaning of $\mathbf{n}$. We will soon find $\mathbf{n}$ to be a key parameter to the problem which is easily found using least squares.

Given a collection of n horizon measurements, $\mathbf{n}$ is seen to be the solution to a simple linear least squares problem

$$\begin{bmatrix}\bar{\mathbf{s}}_1^{'T}\\ \bar{\mathbf{s}}_2^{'T}\\ \vdots\\ \bar{\mathbf{s}}_n^{'T}\end{bmatrix}\mathbf{n} = \begin{bmatrix}1\\1\\\vdots\\1\end{bmatrix} \qquad \text{where} \quad \mathbf{H} = \begin{bmatrix}\bar{\mathbf{s}}_1^{'T}\\ \bar{\mathbf{s}}_2^{'T}\\ \vdots\\ \bar{\mathbf{s}}_n^{'T}\end{bmatrix} \quad \text{and} \quad \mathbf{Hn} = \mathbf{1}_{n\times 1} \tag{46}$$

The vector $\mathbf{n}$ contains *all* the information necessary to compute the position of the spacecraft relative to the planet in square root factorized space. Suppose we write the spacecraft position in square root factorized space in terms of direction and magnitude.

$$\bar{\mathbf{r}} = \bar{\rho}\,\mathbf{e} \tag{47}$$

From simple geometry, we see that*

$$\bar{\rho} = 1/\sin\left(\bar{\phi}\right) \tag{48}$$

*The $1/\sin\bar{\phi}$ scaling of range in the context of horizon-based OPNAV was observed by Battin as early as the 1960s.[9]

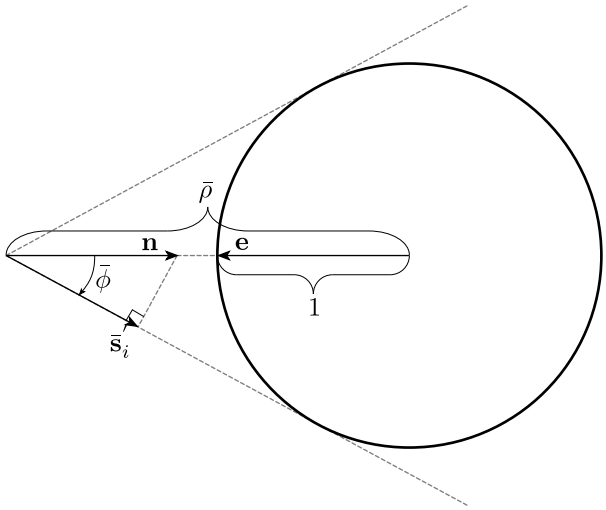

Figure 6. Geometric meaning of n.

Thus, the spacecraft position in square root factorized space can be described by just the cone's centerline direction and half angle,

$$\bar{\mathbf{r}} = \frac{1}{\sin\left(\bar{\phi}\right)}\mathbf{e} \tag{49}$$

Now, it is straightforward to obtain both $\mathbf{e}$ and $\bar{\phi}$ from the definition of $\mathbf{n}$ in Eq. 44

$$\mathbf{e} = -\frac{\mathbf{n}}{\|\mathbf{n}\|} = -\frac{\mathbf{n}}{\sqrt{\mathbf{n}^T\mathbf{n}}} \qquad \|\mathbf{n}\| = \sqrt{\mathbf{n}^T\mathbf{n}} = \frac{1}{\cos\left(\bar{\phi}\right)} \tag{50}$$

Rather than dealing with the angle $\bar{\phi}$ directly, we find it more efficient to use only inner products of $\mathbf{n}$. Observing that

$$\mathbf{n}^T\mathbf{n} = \frac{\bar{\mathbf{r}}^T\bar{\mathbf{r}}}{\bar{\rho}^2\cos^2\left(\phi\right)} = \frac{1}{\cos^2\left(\bar{\phi}\right)} \tag{51}$$

we see that

$$\sin^2\left(\bar{\phi}\right) = 1 - \frac{1}{\mathbf{n}^T\mathbf{n}} \tag{52}$$

or, perhaps more importantly,

$$\bar{\rho} = \frac{1}{\sin\left(\bar{\phi}\right)} = \left(\frac{\mathbf{n}^T\mathbf{n}}{\mathbf{n}^T\mathbf{n} - 1}\right)^{\frac{1}{2}} \tag{53}$$

Therefore, substituting Eq. 50 and Eq. 53 into Eq. 47, we obtain an estimate for $\bar{\mathbf{r}}$,

$$\bar{\mathbf{r}} = \bar{\rho}\,\mathbf{e} = -\left(\frac{\mathbf{n}^T\mathbf{n}}{\mathbf{n}^T\mathbf{n} - 1}\right)^{\frac{1}{2}} \frac{\mathbf{n}}{\sqrt{\mathbf{n}^T\mathbf{n}}} \tag{54}$$

which simplifies to

$$\bar{\mathbf{r}} = -\left(\mathbf{n}^T\mathbf{n} - 1\right)^{-\frac{1}{2}}\mathbf{n} \tag{55}$$

And, finally, transforming back from square root factorized space to the real world using Eq. 41,

$$\mathbf{r} = \mathbf{U}^{-1}\,\bar{\mathbf{r}} = -\left(\mathbf{n}^T\mathbf{n} - 1\right)^{-\frac{1}{2}}\mathbf{U}^{-1}\,\mathbf{n} \tag{56}$$

This non-interative solution allows for the problem to be solved using only a small fraction of the computational effort required for the iterative solutions outlined in the previous solution. Furthermore, this solution leads to a for convenient representation of the solution covariance.

SOLUTION COVARIANCE

The covariance of the non-iterative technique introduced above is identical to that of IHR.[3,4] This is as expected since they are both optimal least squares solutions to the exact horizon-based OPNAV problem — all that differs is their formulation. Thus the non-iterative approach described here solves the OPNAV problem with the same statistical performance but without requiring iteration.

From Eq. 46, it is straightforward to find the covariance of $\mathbf{n}$ as

$$\mathbf{P_n} = \left(\mathbf{H}^T\mathbf{R_y}^{-1}\mathbf{H}\right)^{-1} \tag{57}$$

where $\mathbf{R_y}$ is an $n \times n$ matrix describing the covariance of the residuals,

$$\mathbf{R_y} = \text{diag}\left[\sigma_{y_1}^2,\, \sigma_{y_1}^2, \ldots, \sigma_{y_n}^2\right] \tag{58}$$

Each entry in this covariance matrix is given by

$$\sigma_{y_i}^2 = \mathbf{JUR_sU}^T\mathbf{J}^T \tag{59}$$

where

$$\mathbf{J} = \frac{1}{|\bar{\mathbf{s}}_i|}\left(\mathbf{I}_{3\times 3} - \bar{\mathbf{s}}_i'\bar{\mathbf{s}}_i'^T\right) \tag{60}$$

and $\mathbf{R_s}$ is the covariance of the horizon measurements and can be well approximated as[3]

$$\mathbf{R}_{\mathbf{s}_i} \approx \left(\frac{\sigma_{pix}}{d_x}\right)^2 \begin{bmatrix} 1 & 0 & 0 \\ 0 & 1 & 0 \\ 0 & 0 & 0 \end{bmatrix} \tag{61}$$

where σ_{pix} is the standard deviation of an observed horizon point in units of pixels.

With the covariance of $\mathbf{n}$ known, it is straightforward to find the covariance of $\mathbf{r}$ using Eq. 56,

$$\mathbf{P_r} = \mathbf{FP_nF}^T \tag{62}$$

where

$$\mathbf{F} = -(\mathbf{n}^T\mathbf{n} - 1)^{-\frac{1}{2}}\mathbf{U}^{-1}\left(\mathbf{I}_{3\times 3} - \frac{\mathbf{nn}^T}{\mathbf{n}^T\mathbf{n} - 1}\right) \tag{63}$$

Although space prohibits showing this here, we have shown that the OPNAV covariance from Eq. 62 is identical that first presented by Christian[3] and later parameterized by Hikes and Christian.[4] Thus the analytic uncertainty associated with the non-iterative solution in square root factorized space is identical to that of IHR.

CONCLUSION

This paper explores a number of key geometric properties of the horizon-based OPNAV problem. We first demonstrate that horizon-based OPNAV is a conic section problem and then present a novel method for transforming *all* problems into navigation relative to a unit sphere. These new geometric insights are used to develop a non-iterative solution that works for even highly elliptical planets viewed from an arbitrary vantage point. The performance is shown to be identical to the result obtained by the latest iterative methods. As a result, the geometric insights presented here have led to a substantial advancement in the fundamental theory of horizon-based OPNAV.

ACKNOWLEDGEMENTS

John Christian's portion of this work was made possible by NASA under award NNX13AJ25A.

REFERENCES

[1] J. Christian and E. Lightsey, "Onboard Image-Processing Algorithm for a Spacecraft Optical Navigation Sensors System," *Journal of Guidance, Control, and Dynamics*, Vol. 49, No. 2, 2012, pp. 337–352.

[2] J. Christian, "Optical Navigation Using Planet's Centroid and Apparent Diameter in Image," *Journal of Guidance, Control, and Dynamics*, Vol. 38, No. 2, 2015, pp. 192–204.

[3] J. A. Christian, "Optical Navigation using Iterative Horizon Reprojection," *Journal of Guidance, Control, and Dynamics*, 2016.

[4] J. Hikes and J. A. Christian, "Parametric Covariance Model for Horizon-Based Optical Navigation," *AAS Space Flight Mechanics Meeting*, No. AAS Paper 16-441, Napa, CA, February 2016.

[5] S. Borissov and D. Mortari, "Optimal Single-Point and Filtered Pose Estimation for Lunar Orbiters Using Visible Camera," *24th AAS/AIAA Space Flight Mechanics Meeting*, No. AAS 14-247, Santa Fe, NM, January 2014.

[6] D. Mortari, F. de Dilectis, and R. Zanetti, "Position Estimation Using the Image Derivative," *Aerospace*, Vol. 2, No. 3, 2015, pp. 435–460.

[7] J. A. Christian, J. Hikes, and L. Benhacine, "Geometric Calibration of the Orion Optical Navigation Camera using Star Field Images," *AAS Guidance, Navigation, and Control Conference*, Breckenridge, CO, February 2016.

[8] Y. Ma, S. Soatto, J. Košecká, and S. Sastry, *An Invitation to 3-D Vision: From Images to Geometric Models*, pp. 49–59. New York, NY: Springer, 2010.

[9] R. H. Battin, *Astronautical Guidance*. McGraw-Hill, 1964.